International Journal of Research in Education Humanities and Commerce

Volume 04, Issue 03 "May - June 2023"

ISSN 2583-0333

QUANTITATIVE ANALYSIS OF URBAN GREEN SPACE AND LOCAL COOLING INTENSITY: A CASE STUDY OF CALABAR MUNICIPALITY, NIGERIA

DAPO OLATUNBOSUN[1]*, DICKSON EBONG[1], MAYOWA BANKOLE[2, 3], FRANK ADEJOH[1], CHINEDU OBASI[1], TIJESUNI OGUNROMBI[1, 4]

[1*]Advanced Space Technology Applications Laboratory Uyo, National Space Research and Development Agency, Nigeria

[2]Physical and Life Sciences, National Space Research and Development Agency, Abuja, Nigeria

[3]Department of Microbiology, University of Abuja, Federal Capital Territory, Abuja Nigeria

[4]Department of Petroleum Engineering, University of Uyo, Uyo, Akwa Ibom State, Nigeria

ORCID: 0000-0002-2731-8794 (Dapo Emmanuel Olatunbosun)
0009-0004-2020-717X (Mayowa Bankole)
0000-0001-8099-6626 (Dickson Ebong)
0009-0001-4227-4785 (Frank Adejoh)
0000-0001-9518-6941 (Chinedu Obasi)
0000-0002-1527-1837 (Tijesuni Ogunrombi)

https://doi.org/10.37602/IJREHC.2023.4324

ABSTRACT

This study investigates the thermal spatial expanse of green space and its cooling influence on the surrounding Land Surface Temperature (LST) of a densely urbanized area in Calabar Municipality, Nigeria using the Operational Land Imager (OLI) and Thermal Infrared Sensor (TIRS) of Landsat 8 satellite remotely sensed data. Image pre-processing and analyses were implemented using the Environment for Visualizing Images (ENVI) and the Aeronautical Reconnaissance Coverage Geographic Information System (ArcGIS) application software respectively. Further statistical analysis using the Statistical Package for Social Sciences (SPSS) was performed. In addition, the Split Window temperature algorithm was applied to retrieve the LST. It was observed that Urban Green Space has a positive impact on the ambient environment. Statistical analysis reveals that there is a strong positive correlation between distance from the green space outer boundary and surrounding temperature, with a value of 0.935 at < 0.1 significance. This implies that as the distance increases from the green space outer boundary, the temperature difference increases progressively.

Keywords: Satellite Remote Sensing, Geographic Information System, Land Surface Temperature, Urban Heat Islands, Split Window Temperature Algorithm.

1.0 INTRODUCTION

Globally, the quest for urbanization has been the prime driver of the transformation of vegetated expanses into impervious surfaces (Qihao, 2012). This anthropogenic activity, although beneficial to man, introduces an environmental phenomenon termed Urban Heat Islands (UHI) effects (Oke, 1982; Nnah, et al., 2021). UHI occurs when surface temperature and air are hotter compared to their rural surroundings (Gartland, 2008). In addition, UHI develops due to the radiative, thermal, and moisture properties of urban constructs such as

rooftops and roads that make it possible to take in heat at the surface (Oke, et al., 2017). In cities, research shows that land surface temperatures and air temperatures have the same pattern of expressions (Long & Yong, 2019). The associated UHI heatwave effect could pose bizarre heat stress on urban organisms (Sharon, et al., 2006) and trigger significant heat-related health risks for the residents (Jianquan, et al., 2020). Additionally, there is a negative correlative relationship between vegetation and land surface temperature: this implies that, as the vegetation cover of the land surface increases, the land surface temperature decreases (Oloyede, et al., 2021).

Studies show that vegetation or urban green space (UGS) has been widely used to mitigate the UHI effect due to its cooling counter effect via evapotranspiration and shading (Ranhao & Liding, 2017). Research suggests that the UHI phenomenon is broadly the result of less evapotranspiration—that is when water evaporates from plants or soil into the atmosphere, cooling the air, compared with their surrounding environments. However, other influencers such as the density of the city, the types of building materials and the urban designs incorporated can also play a role (Harvey, 2019). Further, heat exchange and air movement permit green spaces to cool their surroundings (Gómez-Baggethun & Barton, 2013). Global average data predicts that UHI warming will probably be equivalent to about half the warming caused by climate change by the year 2050. Therefore, cities that experience 2 degrees of warming from climate change, would incur an extra degree of warming (Mukul Tewari, 2019). In addition, an upsurge in UHI effects disturbs water-stressed areas as occupants request more water to address outdoor needs (Gober, et al., 2012).

Different degrees (1-7°C) of cooling effects by UGS were reported by various studies using ground truth temperature measurements (Oliveira, et al., 2011; Shashua-Bar, et al., 2009). This ground-based retrieval of temperature data could limit the size of the study area and also increase the design cost (Feyisa, et al., 2014). However, earth observation satellite-based remote sensors data provide high-resolution imagery that covers a huge expanse of land thereby reducing the time and cost of manual temperature retrieval. Also, satellite imagery provides a holistic view of the study area and ensures proper identification of suitable UGS and further analysis.

In this research, we assessed the cooling spatial expanse of urban green space vis-a̓-vis land surface temperature (LST) in Calabar Municipality, Cross River State, Nigeria. Using 2021 Landsat 8-Operational Land Imager & Thermal Infrared Sensor (OLI & TIRS) satellite data, maps were produced that identified suitable urban green space and its spatial cooling extent. LST and vegetation data were used to assess the green space cooling effects. Although weather data from the National Aeronautics and Space Administration (NASA) repository is readily available, research shows that they are not precise (Oloyede, et al., 2022) therefore; ground truth data from the Nigerian Meteorological Agency (NiMet), Calabar Airport station was used in the Split Window temperature retrieval algorithm. Section 2 of this work gives details of the study area considered, while section 3 is the methodology employed. Results and discussion of the results obtained are presented in section 4, accordingly, the conclusion and recommendation are contained in section 5.

2.0 STUDY AREA

The study area includes the area within the boundary of Calabar Municipality, a local government area located in the Southern Senatorial district of Cross River State, Nigeria. It is in the tropical rainforest belt of Nigeria, between latitude 4° 55' 22.16"N and 5° 5' 1.03"N, longitude 8° 15' 5.03"E and 8° 23' 31.82"E. It has a land coverage area of 158.87 sq.km. This cosmopolitan city is selected due to rapid urbanization and the presence of urban green spaces, which are requirements for this analysis. It is important to note also that the study area houses the Nigerian Meteorological Agency (NiMet) and Calabar Airport, which was where ground truth meteorological data was obtained. Under Köppen's climate classification, Calabar features a tropical monsoon climate, with average high air temperatures ranging from 25°C to 28°C. Figure 1 depicts the map of the study area, Calabar Municipality, Cross River State, and Nigeria at large.

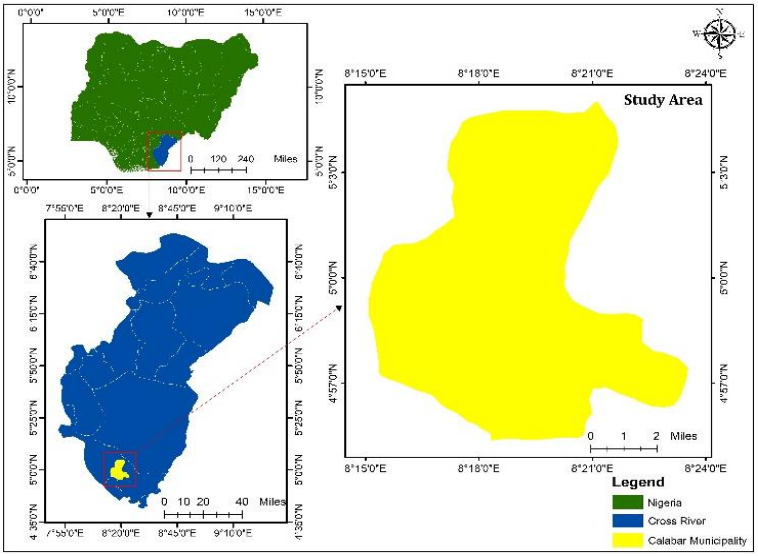

Figure 1: Map Showing Location of the Study Area

3.0 METHODOLOGY

Methods employed for this study are grouped into four stages: 1) Generation of land use/land cover map, 2) Generation of urban green space map, 3) Generation of land surface temperature map, 4) Determination of green space cooling effect distribution.

Remote Sensing Imagery used for this study is the Landsat 8 Operational Land Imager (OLI) and Thermal Infrared (TIRS) sensor data dated 18th February 2021, retrieved from the United State Geological Survey (USGS) repository. Image pre-processing and analyses were implemented using the Environment for Visualizing Images (ENVI) and the Aeronautical Reconnaissance Coverage Geographic Information System (ArcGIS) respectively. Further statistical analyses were done using the Statistical Package for Social Sciences (SPSS).

3.1 Generation of Land Use/Land Cover (LULC) Map

ENVI Support Vector Machine algorithm for supervised classification (Arun, et al., 2012; Mahmoud, 2017) was used to generate the land use/land cover map of Calabar Municipality.

Each pixel was classified into one of four land use/land cover categories – vegetation, built-up, water bodies, and bare land as shown in Figure 2.

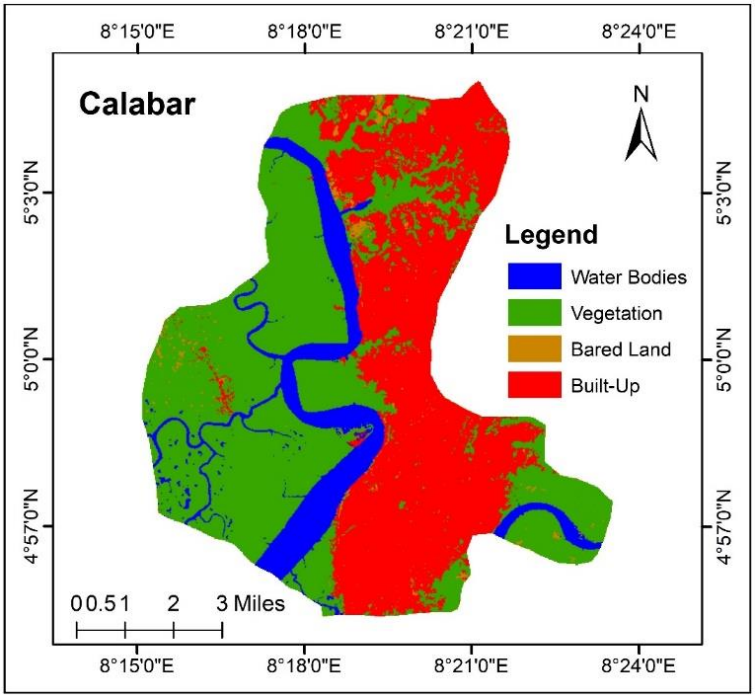

Figure 2: Land Use/Land Cover Map of the Calabar Municipality

3.2 Retrieval of Land Surface Temperature (LST)

The Split-Window Algorithm (SWA) by Tasya et al. (2018) was used to retrieve the LST of the study area. The SWA uses the difference in the atmospheric absorbance of two adjacent long wave infra-red bands to accurately retrieve the LST (Jiménez-Muñoz, et al., 2014). Utilization of two separate thermal bands has been demonstrated to minimize error in the retrieval of LST (Caselles, et al., 1998). TIRS measures the land surface temperature at 100m resolution using Band 10 and 11 located in the atmospheric window between 10 - 12µm (Irons, et al., 2012). The crux of the technique is that the radiance offset for atmospheric absorption is proportional to the radiance difference of simultaneous measurements at two different wavelengths, each of them being subject to different amounts of atmospheric absorption (Sobrino, et al., 2008). The LST was retrieved using the mathematical equation presented in Equation 1 (Jiménez-Muñoz, et al., 2014), proposed by Sobrino et al. (1996).

$$LST=TB10+C1\ (TB10-TB11)+C2\ (TB10-TB11)2+C0\ (C3+C4W)\ (1-\varepsilon)+(C5+C6W)\ \Delta\varepsilon \quad \text{(Equation 1)}$$

Where;

LST is Land Surface Temperature (K),

C0 to C6 are Split-Window Coefficient values, as shown in Table 1,

TB10 and TB11 are the brightness temperatures of band 10 and band 11 (K),

ε is the mean LSE of TIR bands,

W is the atmospheric water vapor content,

Δε is the difference in LSE

An important parameter in the SWA algorithm is the atmospheric water vapor content (W) of the study area, which can be calculated using air humidity and air temperature from a weather station. The input data used was obtained from the NiMet Calabar Airport Station (Lat. 04°58', Long. 08°21') (NiMet, 2022). The meteorological data obtained from NiMet is such that, it has corresponding spatio-temporal resolution with that of the satellite imagery used. Thus, W in the atmosphere column up to satellite altitude can be estimated as presented in Equation 2 (Fei, et al., 2015):

$$W = \frac{w(0)}{R_w(0)} \qquad \text{(Equation 2)}$$

Where;

W is the water vapor content (g/cm-2) in the atmospheric column up to the sensor,

w (0) is the water vapor content (g/cm-2) at the ground of the atmosphere,

R_w (0) is the ratio of water vapor content at the first layer to the total,

Tropical atmosphere has a water vapor ratio R_w (0) = 0.6834 (Qin, et al., 2001)

The water vapor content at the ground level is computed as shown in Equation 3.

$$W(0) = \frac{H \times E \times A}{1000} \qquad \text{(Equation 3)}$$

Where;

H is Air Humidity (%),

E is the saturation mix ratio (g/kg) of water vapor and air for a specific air temperature,

A is the Air Density (kg/m3) at the specific temperature

Table 1 shows the Split-Window coefficient values.

Table 1: SW Coefficient Values

Constant	Value
C0	-0.268
C1	1.378
C2	0.183
C3	54.300

C4	-2.238
C5	-129.200
C6	16.400

3.2.1 Brightness Temperature (TB)

The brightness temperature for both TIRs bands was calculated using the formula presented in Equation 4 (Ogunode & Akombelwa, 2017).

$$TB = K2/\ln(K1/ L\lambda+1) \quad \text{(Equation 4)}$$

Where;

K1 and K2 are thermal conversion constant that varies for the TIR Band 10 and Band 11, as shown in Table 2,

Lλ is the Top of Atmospheric spectral radiance

Table 2 shows the K1 and K2 thermal constants.

Table 2: K1 and K2 Values

Thermal Constant	Band 10	Band 11
K1	774.8853	480.8883
K2	1321.0789	1201.1442

3.2.2 Top of Atmospheric Spectral Radiance (TOA)

The value of Top of Atmospheric (TOA) spectral radiance (Lλ) was determined using the mathematical expression presented in Equation 5 (Fei, et al., 2015).

$$L\lambda = ML * Qcal + AL \quad \text{(Equation 5)}$$

Where;

Lλ is TOA spectral radiance

ML is Radiance multiplicative Band

AL is Radiance Add Band

Qcal is quantized and calibrated standard product pixel values (DN)

The metadata of the satellite imagery is presented in Table 3.

Table 3: Rescaling Factor

Rescaling factor	Band 10	Band 11
ML	0.0003342	0.0003342
AL	0.1	0.1

3.2.3 Land Surface Emissivity (LSE)

Computation of Land Surface Emissivity (LSE) is requisite to estimate Land Surface Temperature. LSE is the average emissivity of an element of the surface of the Earth (Ugur & Gordana, 2016) calculated from the Normalized Difference Vegetation Index (NDVI). LSE is largely dependent on the surface roughness, and the nature of vegetation cover (Javed, et al., 2008). LSE was estimated using the NDVI threshold method, as shown in Equation 6 (Jiménez-Muñoz, et al., 2014).

$$LSE = \varepsilon s * (1-FVC) + (\varepsilon v * FVC) \qquad \text{(Equation 6)}$$

Where;

FVC is Fractional Vegetation Cover,

εs And εv are the Soil and Vegetation Emissivity constants for the TIR Band 10 and Band 11 respectively, as shown in Table 4.

Table 4 shows the emissivity constants of Band 10 and Band 11.

Table 4: Emissivity Constants

Emissivity	Band 10	Band 11
εs	0.971	0.977
εv	0.987	0.989

To calculate Fractional Vegetation Cover, we have to calculate the Normalized Difference Vegetation Index. Equation 7 is used to compute the Fractional Vegetation Cover (Qinqin, et al., 2014).

$$FVC = 〚((NDVI-NDVImin)/(NDVImax-NDVImin))〛^2 \qquad (7)$$

Where;

NDVI is the Normalized Difference Vegetation Index,

NDVImin is the Minimum Normalized Difference Vegetation Index,

NDVImax is the Maximum Normalized Difference Vegetation Index

3.2.4 Normalized Differences Vegetation Index (NDVI)

This indicator serves as a gauge for lush, healthy vegetation. NDVI is computed on per-pixel basis as the normalized difference between the near-infrared band (NIR) and red band (RED) of the images using the formula, as shown in Equation 8 (Zaitunah, et al., 2018).

$$NDVI = (NIR-RED)/(NIR+RED) \qquad \text{(Equation 8)}$$

Where;

NIR is a pixel's near-infrared band value,

RED is the same pixel's red band value

Estimating NDVI is essential since the amount of vegetation present is a factor for LST retrieval (Weng, et al., 2014).

3.2.5 Mean and Difference LSE

Haven generated the LSE for both bands of the TIR, the mean and difference LSE of both bands combined was calculated using Equation 9 (Shaohua, et al., 2009) and Equation 10 (Skokovic, et al., 2014).

$$\varepsilon = (LSE10+LSE11)/ 2 \qquad \text{(Equation 9)}$$

Where;

LSE10 is Band 10 Land Surface Emissivity

LSE11 is Band 10 Land Surface Emissivity

$$\Delta\varepsilon=LSE10-LSE11 \qquad \text{(Equation 10)}$$

Where;

ε is the Mean LSE

$\Delta\ \varepsilon$ is the LSE difference

Finally, the LST in kelvin was determined using SW algorithm and further converted to degree Celsius. Figure 3 depicts the flowchart of LST retrieval.

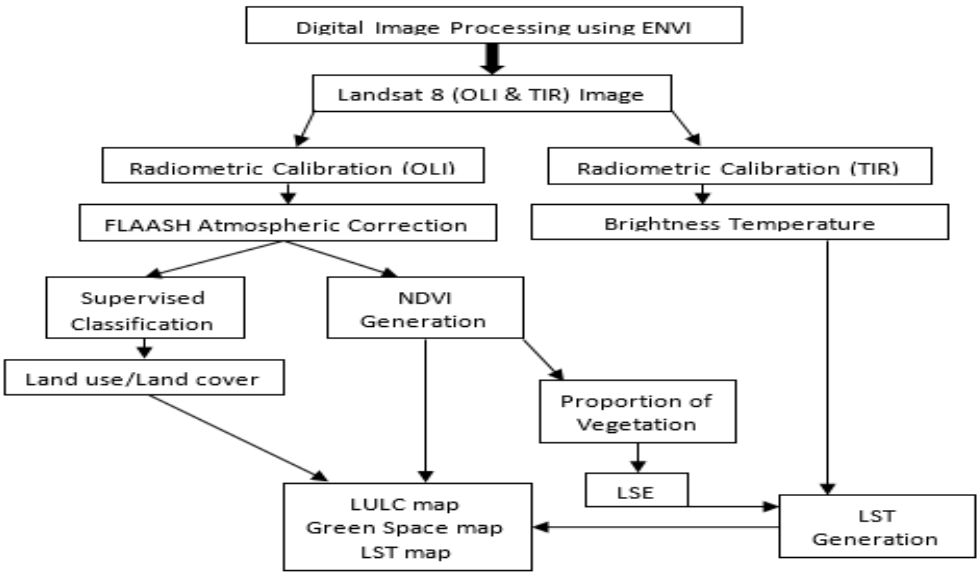

Figure 3: Flowchart for LST Retrieval

3.2.6 Green Space Cooling Spatial Extent

Park Cooling Intensity (PCI) method is used to explore the impact of green space cooling effect on the surrounding environment. PCI calculates the temperature difference between the inside and outside of the park. It could be air temperature or land surface temperature. In this study, the PCI was defined as the mean LST difference (Xin, et al., 2010) as shown in Equation 11.

$$PCI=Tu-Tp \qquad \text{(Equation 11)}$$

Where;

Tu is the mean LST of urban area,

Tp is the mean LST inside the park

To calculate the cooling effect of the green space, we create a series of 30m concentric buffer rings up to 300m originating from the boundary of the green space. Next, calculate the mean LST within each buffer ring and analyse the urban green space cooling effects. Figure 4 shows the selected green space and surrounding area, while Figure 5 shows the LST layer over the green space overlay with the multiple ring buffers. Table 5 is a chart of PCI calculation.

4.0 RESULTS AND DISCUSSION

The 30m buffer interval is considered as suitable distance as it is the size of the pixel of the LST layer, which is 30m. The effective cooling spatial extent of the green space is computed. Green space cooling extent is correlated with the buffer distance to determine the relationship between these two attributes.

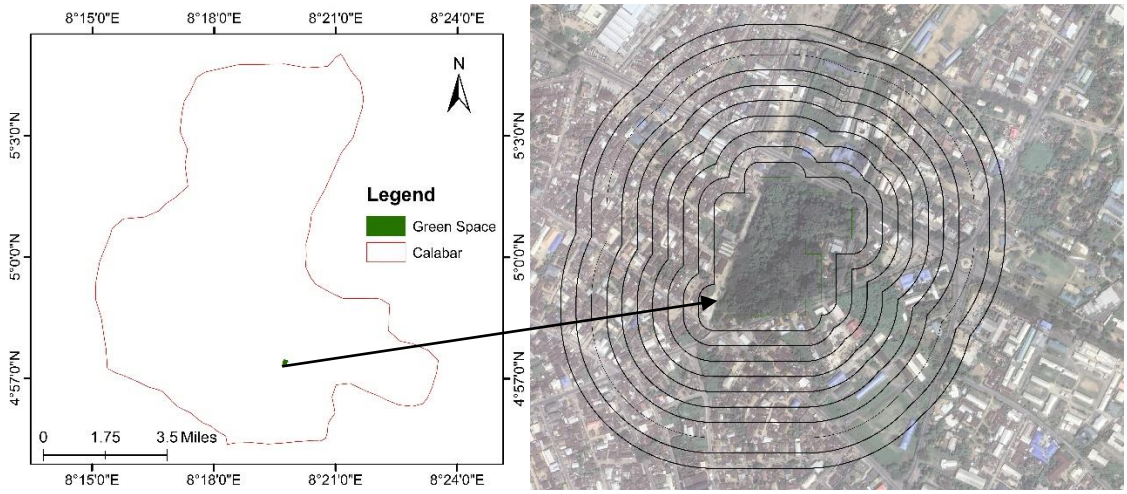

Figure 4: (a) Urban Green Space (b) Google Earth Aerial View of the Suitable Green Space and Surrounding Area with 30m Concentric Multiple Buffer Rings

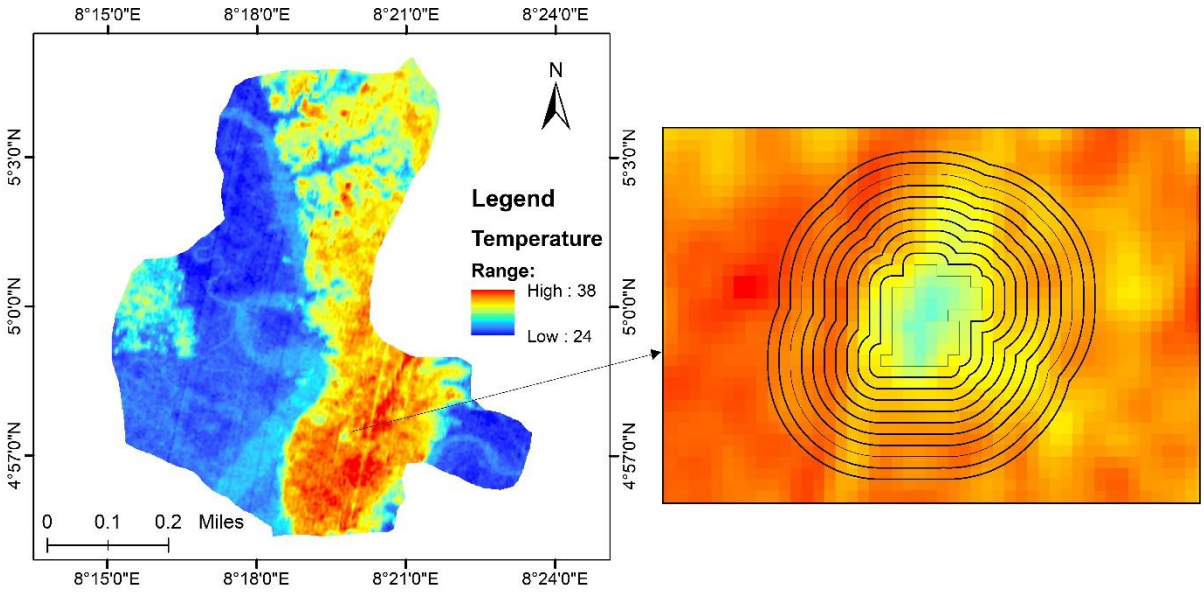

Figure 5: Multiple Buffer Rings Overlay onto LST Layer to Calculate the Green Space Cooling Intensity

Table 5: PCI Chart

Tu (°C)	Tp (°C)	PCI (°C)	Distance From Green Space Boundary (m)
32.75		1.43	30
33.32		2	60
33.93		2.61	90
34.47		3.15	120
34.78	31.32	3.46	150
34.97		3.65	180
35		3.68	210
35.16		3.84	240
35.3		3.98	270
35.43		4.11	300

The study area, which is Calabar Municipality, Cross River State, Nigeria is shown in Figure 1. Satellite imagery (LandSat 8 data of 2021-02-18; Path/Row: 188/56) was downloaded from USGS website and used for this study. The features of the study area chosen includes vegetation cover, water body, built-up area and bare land as shown in Figure 2. After image pre-processing, supervised classification, NDVI and LST analysis were carried out and maps were composed and presented. Figure 5 shows the LST over the study area. Green space located in a densely populated area was mask out of the NDVI as depicted in Figure 4a. The green space has an area of 4.68Ha. The mean temperature within the urban green space boundary is 31.32°C.

4.1 Retrieval of LST Values of green space and surroundings

The LST layer is converted to point values (each raster pixel is represented with a point that averages the raster value). Multiple buffer rings of an interval of 30m distance were generated around the outer boundary of the green space and selection by location was carried out to retrieve the LST point's values within each buffer zone and the mean value of each zone was obtained. Further statistical analysis shows that there is a strong positive correlation value of 0.935 at < 0.1 significance between distance from the green space outer boundary and surrounding temperature, as presented in Figure 6. This implies that as the distance increase from the green space outer boundary, the temperature difference increases progressively. Therefore, the cooling intensity of the green space decreases with increasing distance from its boundary and eventually equilibrate with the surrounding, although with temperature spikes in some areas. This is presented in Figure 7.

		Distance(m)	Park Cooling Intensity
Distance(m)	Pearson Correlation	1	.935**
	Sig. (2-tailed)		.000
	N	10	10
Park Cooling Intensity	Pearson Correlation	.935**	1
	Sig. (2-tailed)	.000	
	N	10	10

**. Correlation is significant at the 0.01 level (2-tailed).

Figure 6: Screenshot of Correlation between PCI and Distance

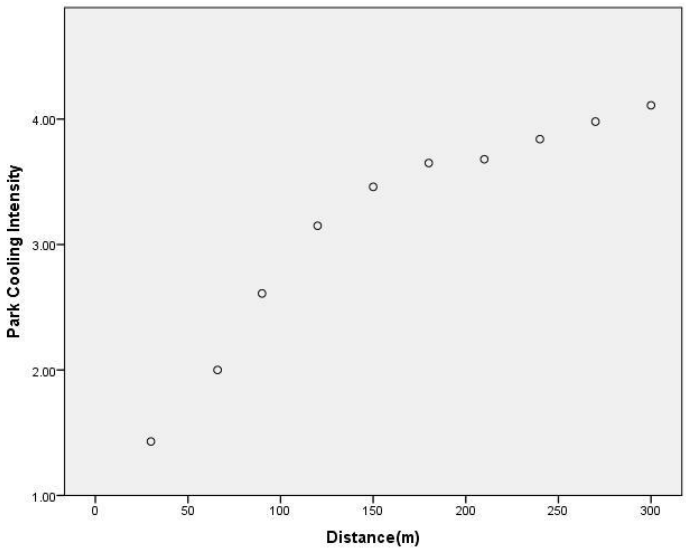

Figure 7: PCI vs Distance

5.0 CONCLUSION AND RECOMMENDATION

It is postulated that urban heat island heatwave poses bizarre heat stress on organisms and by extension triggers significant heat-related health hazards for the residents and the environment. This study has shown that vegetation has an impact on the land surface temperature of the environment, especially urban green spaces, which have a positive impact on the ambient

environment. Urban green spaces should be the new normal in our environs, as their presence will ease the impact of increased land surface temperature in non-vegetated (built-up) urban areas and this will trickle down to improve public health well-being. Further ground truth assessment is required to validate the results acquired from satellite imagery.

Acknowledgements Immense gratitude to management and staff of the National Space Research and Development Agency (NASRDA), the Advanced Space Technology Applications Laboratory Uyo (ASTAL Uyo), Digital Image Processing Laboratory of ASTAL Uyo and the Nigerian Meteorological Agency (NiMet) for their direct and indirect support to this work.

Author's Contribution D.E. Olatunbosun: Conceptualization, Methodology, Image Processing, and Writing – Original draft. A.O. Oloyede: Image Processing, Writing – Review and editing. S.T. Ogunrombi: Software, Writing – Second draft. F.S. Aliu: Validation, Writing – Second Draft. D.E. Ebong: Validation, Writing – Review and editing. C.D. Obasi: Writing – Review and editing.

Funding the authors declare that no funds, grants, or other support was received during the preparation of this manuscript.

Data availability Data are available upon request to the authors.

Declarations

Conflict of interest Authors have no financial or non-financial interests relevant to the content of this article.

REFERENCES

Ali, M. S. & Doaa, R. J., 2014. Monitoring Vegetation Areas by using Remote Sensing Techniques. International Journal of Computer and Information Technology, 3(2).

ARDEN, B. L., 1981. New Equations for Computing Vapor Pressure and Enhancement Factor. Journal of Applied Meteorology, Volume 20, pp. 1527-1532.

Arun, M. et al., 2012. Comparison of Support Vector Machine and Maximum Likelihood Classification Technique using Satellite Imagery. International Journal of Remote Sensing and GIS, 1(2), pp. 116-123.

Caselles, V., Rubio, E., Coll, C. & Valor, E., 1998. Thermal Band Selection for the PRISM Instrument: 3. Optimal Band Configurations. Journal of Geophysical Research Atmospheres, Volume 103, p. 17057–17067.

Claudio, P., 2013. TOA reflectance and NDVI calculation for Landsat 7 ETM+ images of Sicily. Slovak Republic, s.n., pp. 351-354.

Fei, W. et al., 2015. An Improved Mono-Window Algorithm for Land Surface Temperature Retrieval from Landsat 8 Thermal Infrared Sensor Data. Remote sensing, pp. 4268-4289.

Feyisa, G. L., Dons, K. & Meilby, H., 2014. Efficiency of parks in mitigating urban heat island effect: An example from Addis Ababa. Landscape and Urban Planning, pp. 87-95.

Gartland, L. M., 2008. Heat Islands: Understanding and Mitigating Heat in Urban Areas. Routledge, p. 208.

Gober, P. et al., 2012. TRADEOFFS BETWEEN WATER CONSERVATION AND TEMPERATURE AMELIORATION IN PHOENIX AND PORTLAND: IMPLICATIONS FOR URBAN SUSTAINABILITY. Urban Geography, 33(7), pp. 1030-1054.

Gómez-Baggethun, E. & Barton, D. N., 2013. Classifying and valuing ecosystem services for urban planning. Ecological Economics, pp. 235-245.

Gregory, M. J., 1980. A Simple Procedure for Calculating Atmospheric Water Vapor Concentration. Journal of the Air Pollution Control Association, 30(4), pp. 394-394.

Harvey, C., 2019. Urban heat islands mean warming will be worse in cities. [Online]

Available at: https://www.scientificamerican.com/article/urban-heat-islands-mean-warming-will-be-worse-in-cities/

Irons, J. R., Dwyer, J. L. & Barsi, J. A., 2012. The Next Landsat Satellite: The Landsat Data Continuity Mission. Remote Sensing of Environment, Volume 122, pp. 11-21.

Javed, M., Yogesh, K. & Bharath, B., 2008. Estimation of land surface temperature over Delhi using Landsat-7 ETM+. J. Ind. Geophys. Union, Volume 12, pp. 131 -140.

JIANHUA, H., 2018. A Simple Accurate Formula for Calculating Saturation Vapor Pressure of Water and Ice. JOURNAL OF APPLIED METEOROLOGY AND CLIMATOLOGY, Volume 57, pp. 1265-1272.

Jianquan, D. et al., 2020. Heatwave-induced human health risk assessment in megacities based on heat stress-social vulnerability-human exposure framework. Landscape and Urban Planning, 203(103907).

Jiménez-Muñoz, J. C. et al., 2014. Land Surface Temperature Retrieval Methods From Landsat-8 Thermal Infrared Sensor Data. IEEE Geoscience and Remote Sensing Letters, 11(10), pp. 1840-1843.

Long, L. & Yong, Z., 2019. Satellite-Based Spatiotemporal Trends of Canopy Urban Heat Islands and Associated Drivers in China's 32 Major Cities. Remote Sensing, 11(102).

Mahmoud, S., 2017. A survey of modern classification techniques in remote sensing for improved image classification. Journal of Geomatics, 11(1).

Mukul Tewari, J. Y. H. K. F. S. C. W. a. L. T., 2019. Interaction of urban heat islands and heat waves under current and future climate conditions and their mitigation using green and cool roofs in New York City and Phoenix, Arizona. Environmental Reearch Letters.

NiMet, 2022. Nigerian Meteorological Agency. [Online] Available at: https://nimet.gov.ng [Accessed 5 July 2022].

Nnah, B. C. et al., 2021. Geospatial Assessment of Urban Heat Island in Port Harcourt L.G.A, Rivers State, Nigeria. International Journal of Sciences: Basic and Applied Research (IJSBAR), pp. 33-55.

Ogunode, A. & Akombelwa, M., 2017. An algorithm to retrieve Land Surface Temperature using Landsat-8 Dataset. South African Journal of Geomatics, 6(2).

Oke, T. R., 1982. The energetic basis of the urban heat island. QUARTERLY JOURNAL OF THE ROYAL METEOROLOGICAL SOCIETY, 108(455), pp. 1-24.

Oke, T. R., Gerald, M., Andreas, C. & James, A. V., 2017. Urban Climate. Cambridge: Cambridge University Press.

OLEG, A. A. & ROBERT, E. E., 1996. Improved Magnus's form approximation of saturation vapor pressure. JOURNAL OF APPLIED METEOROLOGY, Volume 35, pp. 601-609.

Oliveira, S., Andrade, H. & Vaz, T., 2011. The cooling effect of green spaces as a contribution to the mitigation of urban heat: A case study in Lisbon. Building and Environment, pp. 2186-2194.

Oloyede, A. O. et al., 2021. Correlation Analysis of Vegetation and Land Surface Temperature in Uyo, Nigeria Using Satellite Remote Sensing and Python-Based Geographic Information System. Science and Technology Publishing, 5(2632-1017).

Oloyede, A., Ozuomba , S. & Asuquo, P., 2022. Descriptive and Diagnostic Analysis of NASA and NiMet Big Weather Data. Lagos, Nigeria, IEEE, pp. 1-5.

Qihao, W., 2012. Remote sensing of impervious surfaces in the urban areas: Requirements, methods, and trends. Remote Sensing of Environment, Volume 117, pp. 34-49.

Qinqin, S., Jianjun, T. & Yonghang, X., 2014. An ERDAS image processing method for retrieving LST and describing urban heat evolution: a case study in the Pearl River Delta Region in South China. Environ Earth Sci, Volume 59, pp. 1047 - 1055.

Qin, Z., Karnieli, A. & Berliner, P., 2001. A Mono-Window Algorithm for Retrieving Land Surface Temperature from Landsat TM data and its Application to the Israel-Egypt Border Region. International Journal of Remote Sensing, 22(18), pp. 3719-3746.

Ranhao, S. & Liding, C., 2017. Effects of green space dynamics on urban heat islands: Mitigation and diversification. Ecosystem Services, 23(2212-0416), pp. 38-46.

Shaohua, Z. et al., 2009. Comparison of two split-window methods for retrieving land surface temperature from MODIS data. J. Earth Syst. Sci, 118(4), pp. 345-353.

Shaohua, Z. et al., 2009. Comparison og two Split-Window Mehtods for Retrieving Land Surface Temperature from MODIS Data. Journal of Earth Syst. Science, 118(4), pp. 345-353.

Sharon, H. L. et al., 2006. Neighborhood microclimates and vulnerability to heat stress. Social Science & Medicine, 63(11), pp. 2847-2863.

Shashua-Bar, L., Pearlmutter, D. & Erell, E., 2009. The cooling efficiency of urban landscape strategies in a hot dry climate. Landscape and Urban Planning, pp. 179-186.

Skokovic, D. et al., 2014. Calibration and Validation of Land Surface Temperature for Landsat 8 – TIRS Sensor. Land product Validation and Evolution, ESA/ESRIN Frascati (Italy), pp. 6-9.

Sobrino, J. A. et al., 2008. Land Surface Emissivity Retrieval from Different VNIR and TIR Sensors. IEEE Transactions on Geoscience and Remote Sensing, 46(2).

Sobrino, J. A., Li, Z.-L., Stoll, M. P. & Becker, F., 1996. Multi-channel and multi-angle algorithms for estimating sea and land surface temperature with ATSR data. International Journal of Remote Sensing, 17(11), pp. 2089-2114.

Tasya, B., Rokhmatuloh & Adi, W., 2018. Comparison Spatial Pattern of Land Surface Temperature with Mono Window Algorithm and Split Window Algorithm: A Case Study in South Tangerang, Indonesia. s.l., s.n.

Ugur, A. & Gordana, J., 2016. Algorithm for Automated Mapping of Land Surface Temperature Using LANDSAT 8 Satellite Data. Journal of Sensors.

Weng, Q., Fu, P. & Gao, F., 2014. Generating daily land surface temperature at Landsat resolution by fusing Landsat and modis data. Remote sensing of environment, Volume 145, pp. 55-67.

Xiaoyun, C. et al., 2014. Influence of Park Size and Its Surrounding Urban Landscape Patterns on the Park Cooling Effect. J. Urban Plann. Develop, 141(3).

Xin, C., Akio, O., Jin, C. & Hidefumi, I., 2010. Quantifying the cool island intensity of urban parks using ASTER and IKONOS data. Landscape and Urban Planning, Volume 96, pp. 224-231.

Zaitunah, A., Samsuri, A., Ahmad, G. & Safitri, R. A., 2018. Normalized difference vegetation index (ndvi) analysis for land cover types using landsat 8 oli in besitang watershed, Indonesia. s.l., s.n.

Zhao-Liang, L., Becker, F., Stoll, M. P. & Zhengming, W., 1999. Evaluation of Six Methods for Extracting Relative Emissivity Spectra from Thermal Infrared Images. Remote sensing of Environment, 69(3), pp. 197-214.

